Available online at www.sciencedirect.com
ScienceDirect
Journal of Sound and Vibration 309 (2008) 588–599
JOURNAL OF SOUND AND VIBRATION
www.elsevier.com/locate/jsvi

Geometric effects on thermoelastic damping in MEMS resonators

Y.B. Yi*

Department of Mechanical and Materials Engineering, University of Denver, Denver, CO 80208, USA

Received 25 August 2006; received in revised form 19 July 2007; accepted 24 July 2007
Available online 10 September 2007

Abstract

The effects of geometry on the energy dissipation induced by thermoelastic damping in MEMS resonators are investigated numerically using a finite element formulation. The perturbation analysis is applied to derive a linear eigenvalue equation for the exponentially decaying rate of the mechanical oscillation. The analysis also involves a Fourier method that reduces the dimensionality of the problem and considerably improves the computational efficiency. The method is first validated by comparing the two-dimensional model to the existing analytical solutions for a simply supported beam system, and then it is extended to a three-dimensional axisymmetric geometry to obtain the energy loss as a function of the geometric parameters in a silicon ring resonator. The computational results reveal that there is a peak value for the resonant frequency when the radial width of the ring varies. In addition, the quality factor (Q-factor) decreases with the radial width as a monotonic function.

1. Introduction

Modeling and simulation of thermoelastic damping is a recurrent interest in the community of micromechanics and microengineering, mainly motivated by the recent advancement of MEMS (microelectromechanical) and NEMS (nanoelectromechanical) technologies and the associated energy dissipation problems in high performance actuators, resonators and filters [1–4].

The mechanism of thermoelastic damping was first explained by Zener [5] many decades ago. He indicated that the phenomenon is induced by the irreversible heat dissipation during the coupling of heat transfer and strain rate in an oscillating system. He also derived an analytical solution to relate the energy dissipation (i.e. quality factor, Q) and the material properties of a thin beam structure. However, some mathematical and physical simplifications were assumed in this derivation. Lifshitz and Roukes [6] recently refined the theory without involving these simplifications and reported a higher precision solution, although the direct application of the solution was still limited to beam systems. Nayfeh and Younis [7] later extended the technique to solve a problem relevant to microplates, which was believed to have wide applications in micropumps and pressure sensors. Wong et al. [8] further extended the method to investigate the in-plane

*Tel.: +1 303 871 2228; fax: +1 303 871 4450.
E-mail address: yyi2@du.edu

0022-460X/$ - see front matter © 2007 Elsevier Ltd. All rights reserved.
doi:10.1016/j.jsv.2007.07.055

vibration of thin rings (i.e. silicon gyros [9]) and the effect of the three-dimensional (3-D) geometry on the phenomenon was explored for the first time. Recently a research group in the Naval Research Laboratory [10,11] reported some important results regarding the thermoelastic loss in microscale oscillators and they introduced a link between Zener's analytical form for a simple reed in bending and more complicated resonator shapes.

These works were quite successful in predicting the energy dissipation for certain types of MEMS systems. However, all of them used analytical approaches and were thus limited to those simple geometries such as beams and plates of regular shapes. Although Wong et al. [8] studied the resonance of MEMS gyros, their work was focused on the in-plane vibration of thin rings, which was virtually not quite different from the classical beam problems. The rapid advancement of MEMS/NEMS technology these days requires design and fabrication of microstructures with more complex geometry such as micro-mirror systems reported in Guan and Matin's work [12,13]. It is desirable to have a generalized formulation that can systematically explore the geometric effects on the phenomenon of thermoelastic damping. Employing a finite element approach, rather than an analytical approach, is essential for achieving this goal.

Using the finite element method to solve thermoelastic damping problems is actually not new. For example, a finite element formulation was implemented by Gorman [14] using a multiphysics simulation code. Similarly, Silver and Peterson [15] proposed to use a finite element analysis to solve the thermoelastic damping problem for a truss structure in the aerospace industry. In their approach, the problem was formulated in a way similar to a linearly viscoelastic structure. However, the determination of the elastic stiffness matrix needs the evaluation of an augmenting stiffness matrix, which must be expressed in a complicated integral form. So far it is not clear whether the method can be easily extended to solve problems other than beams or trusses.

The present work is focused on 2-D and 3-D continuum solids rather than beam or truss structures, and it employs a different approach in which perturbation forms of the temperature and displacement fields used in the governing equations directly lead to an eigenvalue equation. The eigenvalue is associated with the frequency of the harmonic as well as the decaying rate of the amplitude. Further, the introduction of the Fourier reduction method simplifies the finite element discretization and thus the resulting problem has a reduced order. For example, a 3-D axisymmetric geometry can be reduced to a problem defined on its cross-sectional domain only. This method was adapted from the one used in the eigenvalue solution of the frictionally excited thermoelastic instability (TEI) in automotive disk brakes and clutches [16,17], despite that these two phenomena occur at different size scales and involve different physical mechanisms. Based on this technique, the geometric effect on thermoelastic damping is evaluated and the comparisons are made between the 2-D beams and 3-D rings. The application of the eigenvalue method and the finite element method in conjunction with the Fourier reduction makes it possible a significant enhancement in the computational efficiency for certain types of thermoelastic damping problems.

2. Eigenvalue formulation

2.1. Heat transfer equation

The heat transfer equation involving thermoelastic damping can be written as

$$k\nabla^2 T = \frac{\partial T}{\partial t} + \frac{E\alpha T_0}{(1-2\nu)C_v}\frac{\partial \bar{e}}{\partial t}, \tag{1}$$

where k is the thermal diffusivity, E is the elastic modulus, α is the thermal expansion coefficient, ν is Poisson's ratio, C_v is the heat capacity per unit volume, T_0 is the mean temperature and $\bar{e}$ is the dilatation strain due to the thermal effect:

$$\bar{e} = \varepsilon_{xx} + \varepsilon_{yy} + \varepsilon_{zz}, \tag{2}$$

where ε_{xx}, ε_{yy}, ε_{zz} are the strains in the x, y and z directions. Note that the problem has been linearized in a way such that the temperature T in the thermoelastic coupling term is substituted with the mean absolute temperature T_0.

We assume an exponentially growing perturbation solution of the form

$$\begin{cases} T = \mathrm{Re}\{e^{bt}\Theta\}, \\ u = \mathrm{Re}\{e^{bt}U\}, \\ u' = \mathrm{Re}\{e^{bt}U'\}, \end{cases} \tag{3}$$

where Re represents the real part of a complex number; b is a complex exponential growth rate (or decaying rate, depending on whether it is positive or negative). Applying the standard Galerkin finite element formulation [18] results in a matrix equation for nodal temperature Θ and nodal displacement U in the following form:

$$(\mathbf{K} + b\mathbf{H})\Theta + b\mathbf{F}\mathbf{U} = 0, \tag{4}$$

where $\mathbf{K}$, $\mathbf{H}$ and $\mathbf{F}$ are coefficient matrices.

2.2. Equations of motion and thermoelasticity

The equations of motion for an elastic solid in the absence of body force are as follows:

$$\begin{cases} \dfrac{\partial \sigma_{xx}}{\partial x} + \dfrac{\partial \sigma_{xy}}{\partial y} + \dfrac{\partial \sigma_{xz}}{\partial z} = \rho \dfrac{\partial^2 u_x}{\partial t^2}, \\ \dfrac{\partial \sigma_{xy}}{\partial x} + \dfrac{\partial \sigma_{yy}}{\partial y} + \dfrac{\partial \sigma_{yz}}{\partial z} = \rho \dfrac{\partial^2 u_y}{\partial t^2}, \\ \dfrac{\partial \sigma_{xz}}{\partial x} + \dfrac{\partial \sigma_{yz}}{\partial y} + \dfrac{\partial \sigma_{zz}}{\partial z} = \rho \dfrac{\partial^2 u_z}{\partial t^2}, \end{cases} \tag{5}$$

where σ represent stress; u is displacement; ρ is density. The constitutive law of thermoelasticity is

$$\sigma = \mathbf{C}\varepsilon - \mathbf{D}T. \tag{6}$$

The strain vector ε can be expressed in a matrix form related to the nodal displacement vector $\mathbf{U}$:

$$\varepsilon = \mathbf{B}\mathbf{U}. \tag{7}$$

Consequently the matrix equation of motion becomes

$$\mathbf{L}\mathbf{U} - \mathbf{G}\boldsymbol{\Theta} + b\mathbf{M}\mathbf{U}' = 0. \tag{8}$$

It should be pointed out that by treating the velocity field as a perturbation independent of displacement, the otherwise quadratic eigenvalue equation has been reduced to a linear, first-order eigenvalue problem, which is mathematically much easier to manipulate.

2.3. Eigenvalue equation

There exists a fundamental relationship between the displacement and velocity perturbations as below:

$$\mathbf{U}' = b\mathbf{U}. \tag{9}$$

Combining Eqs. (4), (8) and (9) yields

$$\widetilde{\mathbf{A}}\mathbf{X} = \mathbf{b}\widetilde{\mathbf{B}}\mathbf{X}, \tag{10}$$

where

$$\tilde{\mathbf{A}} = \begin{bmatrix} \mathbf{K} & 0 & 0 \\ \mathbf{G} & -\mathbf{L} & 0 \\ 0 & 0 & \mathbf{I} \end{bmatrix}, \tag{11}$$

$$\tilde{\mathbf{B}} = \begin{bmatrix} \mathbf{H} & \mathbf{F} & 0 \\ 0 & 0 & \mathbf{M} \\ 0 & \mathbf{I} & 0 \end{bmatrix}, \tag{12}$$

$$\mathbf{X} = [\boldsymbol{\Theta}, \mathbf{U}, \mathbf{U}']^{\mathrm{T}} \tag{13}$$

and $\mathbf{I}$ is an identity matrix. This is a generalized eigenvalue equation. The eigenvalue of the equation is the growth rate b and the eigenvector is $[\boldsymbol{\Theta},\mathbf{U},\mathbf{U}']^{\mathrm{T}}$, namely a vector combining nodal temperature, displacement and velocity together.

The effect of thermoelastic damping on the attenuation of the vibration can be expressed in the quality factor Q defined as

$$Q = \frac{1}{2}\left|\frac{\mathrm{Im}(b)}{\mathrm{Re}(b)}\right|, \tag{14}$$

where $\mathrm{Re}(b)$ and $\mathrm{Im}(b)$ represent the real part and the imaginary part of b, respectively. So far the coefficient matrices in the above eigenvalue equation have not been evaluated. Their forms vary for different models. In the following sections, these matrices will be presented separately in each of the models. For brevity, the detail procedures of the derivations are omitted and only the final results are presented.

3. 2-D layer model

A 2-D layer model is referred to as a "layer" having a finite thickness as shown in Fig. 1(a). The layer is assumed either plane-stress or plane-strain and the third dimension (z-axis) is not considered. This model can be used to approximate a beam or plate structure. The resulting elemental matrices in the eigenvalue equation are

$$\mathbf{K}_e = \int_{\Omega} k\left(\frac{\partial \mathbf{N}}{\partial x}\frac{\partial \mathbf{N}^{\mathrm{T}}}{\partial x} + \frac{\partial \mathbf{N}}{\partial y}\frac{\partial \mathbf{N}^{\mathrm{T}}}{\partial y}\right) \mathrm{d}x\,\mathrm{d}y, \tag{15}$$

$$\mathbf{H}_e = \int_{\Omega} C_v \mathbf{N}\mathbf{N}^{\mathrm{T}}\,\mathrm{d}x\,\mathrm{d}y, \tag{16}$$

$$\mathbf{F} = [\,\mathbf{F}_1 \quad \mathbf{F}_2 \quad \mathbf{F}_3 \quad \mathbf{F}_4\,], \tag{17}$$

where

$$\mathbf{F}_i = \frac{E\alpha T_0}{1-2\nu}\mathbf{N}\left[\frac{\mathrm{d}\mathbf{N}_i}{\mathrm{d}x} + \frac{\mathrm{d}\mathbf{N}_i}{\mathrm{d}y} \quad \frac{\mathrm{d}\mathbf{N}_i}{\mathrm{d}x} + \frac{\mathrm{d}\mathbf{N}_i}{\mathrm{d}y}\right] \quad (i = 1,2,3,4), \tag{18}$$

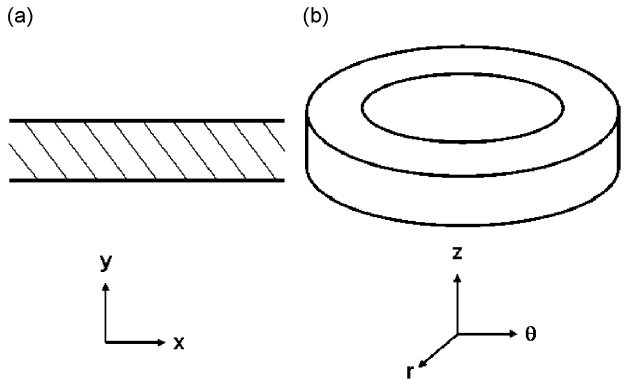

Fig. 1. Two models under investigation: (a) two-dimensional layer model; and (b) three-dimensional annular ring model.

$$\mathbf{B} = [\,\mathbf{B}_1 \quad \mathbf{B}_2 \quad \mathbf{B}_3 \quad \mathbf{B}_4\,] \tag{19}$$

in which

$$\mathbf{B}_i = \begin{bmatrix} \dfrac{\mathrm{d}\mathbf{N}_i}{\mathrm{d}x} & 0 \\ 0 & \dfrac{\mathrm{d}\mathbf{N}_i}{\mathrm{d}y} \\ \dfrac{\mathrm{d}\mathbf{N}_i}{\mathrm{d}y} & \dfrac{\mathrm{d}\mathbf{N}_i}{\mathrm{d}x} \end{bmatrix} \quad (i = 1,2,3,4), \tag{20}$$

$$\mathbf{L}_e = \int_\Omega \mathbf{B}^{\mathrm{T}}\mathbf{C}\mathbf{B}\,\mathrm{d}x\,\mathrm{d}y, \tag{21}$$

$$\mathbf{G}_e = \int_\Omega \mathbf{B}^{\mathrm{T}}\mathbf{D}\mathbf{N}\,\mathrm{d}x\,\mathrm{d}y, \tag{22}$$

$$\mathbf{M}_e = \int_\Omega \rho\mathbf{N}\mathbf{N}^{\mathrm{T}}\,\mathrm{d}x\,\mathrm{d}y. \tag{23}$$

In the above integrals x is the longitudinal direction and y is along the thickness. $\mathbf{N}(x,y)$ is the shape function and $\mathbf{N}_i$ ($i = 1,2,3,4$) represents the four terms in $\mathbf{N}(x,y)$. (The finite elements used in this study are 2-D quadrilateral elements.)

Since this model is based on the general 2-D geometry, arbitrary boundary conditions are applicable such as clamped or simply supported conditions. In addition, insulated thermal conditions are specified on the boundaries since the heat transfer between the material and surroundings is comparably much smaller than the thermal relaxation inside the material.

4. 2-D Fourier model

The formulation of a 2-D Fourier model is similar to the 2-D layer model discussed above. However, the Fourier reduction scheme is applied such that the finite element mesh is generated on the thickness direction only (y-axis). The variation in the longitudinal direction (x-axis) has been canceled in the formulation. However, the resulting model is not simply a 1D problem, since the coefficient matrices are functions of the predefined Fourier number (namely, the wavenumber per unit length). In addition, all the degrees of freedom are retained in the 1D mesh, i.e., they not only possess the y-components of the nodal displacements and velocities, but have the components in the x-direction as well. The application of the Fourier model is restricted to those cases in which the boundary conditions are homogeneous and the layer thickness is uniform, whereas the general 2-D formulation aforementioned does not have this limitation.

Considering a 2-D Fourier model, from the orthogonality analysis we can assume an exponentially growing perturbation solution in the Fourier series along the x-axis, and the solution components for each Fourier number m are

$$\begin{cases} T(x,y,,t) = \mathrm{Re}\{\mathrm{e}^{bt}\Theta(y)\}\cos(my), \\ u_x(x,y,t) = \mathrm{Re}\{\mathrm{e}^{bt}U_x(y)\}\sin(my), \\ u_y(x,y,t) = \mathrm{Re}\{\mathrm{e}^{bt}U_y(y)\}\sin(my), \\ u'_x(x,y,t) = \mathrm{Re}\{\mathrm{e}^{bt}U'_x(y)\}\sin(my), \\ u'_y(x,y,t) = \mathrm{Re}\{\mathrm{e}^{bt}U'_y(y)\}\sin(my), \end{cases} \tag{24}$$

where m is the Fourier number (or wavenumber) defined as the number of oscillations for perturbation within a length of 2π. The reason that the temperature and displacement assume different forms of trigonometry (one is a cosine function, the other is a sine function) is due to the symmetry in the geometry. For example, at a location of the highest temperature, the displacement must be zero. The elemental matrices in the eigenvalue

equation can be expressed as

$$\mathbf{K}_e = \int_\Omega k\left(\frac{\partial \mathbf{N}}{\partial y}\frac{\partial \mathbf{N}^{\mathrm{T}}}{\partial y} + m^2\mathbf{N}\mathbf{N}^{\mathrm{T}}\right)\mathrm{d}y, \tag{25}$$

$$\mathbf{H}_e = \int_\Omega C_v\mathbf{N}\mathbf{N}^{\mathrm{T}}\,\mathrm{d}y, \tag{26}$$

$$\mathbf{F} = \frac{E\alpha T_0}{1-2v}\mathbf{N}\left[\frac{\mathrm{d}\mathbf{N}_1}{\mathrm{d}x} - m\mathbf{N}_1 \quad \frac{\mathrm{d}\mathbf{N}_1}{\mathrm{d}x} + m\mathbf{N}_1 \quad \frac{\mathrm{d}\mathbf{N}_2}{\mathrm{d}x} - m\mathbf{N}_2 \quad \frac{\mathrm{d}\mathbf{N}_2}{\mathrm{d}x} + m\mathbf{N}_2\right], \tag{27}$$

$$\mathbf{B}(m,x) = \begin{bmatrix} \dfrac{\mathrm{d}\mathbf{N}_1}{\mathrm{d}x} & 0 & \dfrac{\mathrm{d}\mathbf{N}_2}{\mathrm{d}x} & 0 \\ 0 & m\mathbf{N}_1 & 0 & m\mathbf{N}_2 \\ -m\mathbf{N}_1 & \dfrac{\mathrm{d}\mathbf{N}_1}{\mathrm{d}x} & -m\mathbf{N}_2 & \dfrac{\mathrm{d}\mathbf{N}_2}{\mathrm{d}x} \end{bmatrix}. \tag{28}$$

The expressions for $\mathbf{L}_e$, $\mathbf{G}_e$ and $\mathbf{M}_e$ remain the same as the 2-D layer model except that the integral variable becomes y rather than both x and y. The expressions for the coefficient matrices $\mathbf{C}$ and $\mathbf{D}$ remain the same.

Since this model is based on the Fourier assumption, it can only be applied to beam or plate problems involving rigorously sinusoidal modes, such as those in simply supported beams and clamped rectangular plates. For the thermal constraints, insulated boundary conditions are specified on the model.

5. 3-D Fourier model

For a 3-D annular ring as shown in Fig. 1(b), the Fourier reduction method leads to a finite element discretization on the 2-D cross-sectional domain of the geometry. Again, all the degrees of freedom are retained in the resulting 2-D mesh and the solution to the problem is a function of the Fourier number (or, the number of oscillations around the ring circumference). We apply the perturbation in the Fourier form as follows:

$$\begin{cases} T(r,\theta,z,t) = \mathrm{Re}\{\mathrm{e}^{bt}\Theta(r,z)\}\cos(n\theta), \\ u_\theta(r,\theta,z,t) = \mathrm{Re}\{\mathrm{e}^{bt}U_\theta(r,z)\}\sin(n\theta), \\ u_r(r,\theta,z,t) = \mathrm{Re}\{\mathrm{e}^{bt}U_r(r,z)\}\cos(n\theta), \\ u_z(r,\theta,z,t) = \mathrm{Re}\{\mathrm{e}^{bt}U_z(r,z)\}\cos(n\theta), \\ u'_\theta(r,\theta,z,t) = \mathrm{Re}\{\mathrm{e}^{bt}U'_\theta(r,z)\}\sin(n\theta), \\ u'_r(r,\theta,z,t) = \mathrm{Re}\{\mathrm{e}^{bt}U'_r(r,z)\}\cos(n\theta), \\ u'_z(r,\theta,z,t) = \mathrm{Re}\{\mathrm{e}^{bt}U'_z(r,z)\}\cos(n\theta). \end{cases} \tag{29}$$

Again, different forms of trigonometry are used for each component due to the symmetries in the geometry. The heat transfer equation associated with thermoelastic damping in a 3-D cylindrical coordinate system is

$$k\left(\frac{\partial^2 T}{\partial r^2} + \frac{1}{r}\frac{\partial T}{\partial r} + \frac{1}{r^2}\frac{\partial^2 T}{\partial \theta^2} + \frac{\partial^2 T}{\partial z^2}\right) = \frac{\partial T}{\partial t} + \frac{E\alpha T_0}{(1-2v)C_v}\frac{\partial \bar{e}}{\partial t}. \tag{30}$$

The elemental matrices can be expressed as

$$\mathbf{K}_e = \int_\Omega k\left(\frac{\partial \mathbf{N}}{\partial r}\frac{\partial \mathbf{N}^{\mathrm{T}}}{\partial r} + \frac{\partial \mathbf{N}}{\partial z}\frac{\partial \mathbf{N}^{\mathrm{T}}}{\partial z} + \frac{n^2}{r^2}\mathbf{N}\mathbf{N}^{\mathrm{T}}\right)\mathrm{d}r\,\mathrm{d}z, \tag{31}$$

$$\mathbf{H}_e = \int_\Omega C_v\mathbf{N}\mathbf{N}^{\mathrm{T}}\,\mathrm{d}r\,\mathrm{d}z, \tag{32}$$

$$\mathbf{F} = [\mathbf{F}_1 \quad \mathbf{F}_2 \quad \mathbf{F}_3 \quad \mathbf{F}_4], \tag{33}$$

$$\mathbf{F}_i = \frac{E\alpha T_0}{1-2\nu}\mathbf{N}\begin{bmatrix} \dfrac{\partial \mathbf{N}_i}{\partial r} + \dfrac{\mathbf{N}_i}{r} - \dfrac{n\mathbf{N}_i}{2r} + \dfrac{1\partial \mathbf{N}_i}{2\,\partial z} \\ \dfrac{n\mathbf{N}_i}{r} + \dfrac{1}{2}\left(\dfrac{\partial \mathbf{N}_i}{\partial r} - \dfrac{\mathbf{N}_i}{r}\right) + \dfrac{1\partial \mathbf{N}_i}{2\,\partial z} \\ \dfrac{\partial \mathbf{N}_i}{\partial z} - \dfrac{n\mathbf{N}_i}{2r} + \dfrac{1\partial \mathbf{N}_i}{2\,\partial r} \end{bmatrix}^{\mathrm{T}} \quad (i = 1,2,3,4), \tag{34}$$

$$\mathbf{C} = \frac{E}{(1+\nu)(1-2\nu)}\begin{bmatrix} 1-\nu & \nu & \nu & 0 & 0 & 0 \\ \nu & 1-\nu & \nu & 0 & 0 & 0 \\ \nu & \nu & 1-\nu & 0 & 0 & 0 \\ 0 & 0 & 0 & 1-2\nu & 0 & 0 \\ 0 & 0 & 0 & 0 & 1-2\nu & 0 \\ 0 & 0 & 0 & 0 & 0 & 1-2\nu \end{bmatrix}, \tag{35}$$

$$\mathbf{D} = \frac{E\alpha}{(1-2\nu)}[1 \quad 1 \quad 1 \quad 0 \quad 0 \quad 0]^{\mathrm{T}}, \tag{36}$$

$$\mathbf{B} = [\mathbf{B}_1 \quad \mathbf{B}_2 \quad \mathbf{B}_3 \quad \mathbf{B}_4], \tag{37}$$

$$\mathbf{B}_i = \begin{bmatrix} \dfrac{\partial \mathbf{N}_i}{\partial r} & 0 & 0 \\ \dfrac{\mathbf{N}_i}{r} & \dfrac{n\mathbf{N}_i}{r} & 0 \\ 0 & 0 & \dfrac{\partial \mathbf{N}_i}{\partial z} \\ -\dfrac{n\mathbf{N}_i}{2r} & \dfrac{1}{2}\left(\dfrac{\partial \mathbf{N}_i}{\partial r} - \dfrac{\mathbf{N}_i}{r}\right) & 0 \\ 0 & \dfrac{1\partial \mathbf{N}_i}{2\,\partial z} & -\dfrac{n\mathbf{N}_i}{2r} \\ \dfrac{1\partial \mathbf{N}_i}{2\,\partial z} & 0 & \dfrac{1\partial \mathbf{N}_i}{2\,\partial r} \end{bmatrix} \quad (i = 1,2,3,4). \tag{38}$$

The expressions for matrices $\mathbf{L}_e$, $\mathbf{G}_e$ and $\mathbf{M}_e$ remain the same as the 2-D layer model except that the integral domain is now on the r–z plane and the cylindrical coordinate system should be used.

Again, since this model is based on the Fourier assumption, it can only be applied to the 3-D problems involving rigorously sinusoidal modes, such as those in annular rings. For the thermal constraints, convection and radiation between the material and surroundings are negligible and therefore insulated boundary conditions are specified.

6. Analytical solutions of the beam problem

Zener's solution [5] for thermoelastic damping in a thin beam can be written in a simplified form as

$$Q^{-1} = \frac{E\alpha^2 T_0}{C_v}\frac{\eta}{1+\eta^2}, \tag{39}$$

where

$$\eta = \frac{\omega_0 h^2}{\pi^2 k} \tag{40}$$

and ω_0 is the undamped natural frequency for the relevant mode; h is the thickness of the beam. For a simply supported beam, the first natural frequency is

$$\omega_0^2 = \frac{\pi^4 E h^2}{12\rho L^4}. \tag{41}$$

Lifshitz and Roukes' exact solution [6] for the same thin beam problem can be expressed in the following form:

$$Q^{-1} = \frac{E\alpha^2 T_0}{c_v}\left(\frac{6}{\xi^2} - \frac{6}{\xi^3}\frac{\sin\,\xi + \sinh\,\xi}{\cos\,\xi + \cosh\,\xi}\right), \tag{42}$$

where

$$\xi = h\sqrt{\frac{\omega_0}{2k}}. \tag{43}$$

7. Results and discussions

The finite element method formulated above was first validated by comparing the quality factor of resonance for a simply supported thin beam between the 2-D models and the existing analytical solutions. In Fig. 2, results obtained from four distinct models are presented together: (1) the 2-D model (non-Fourier model); (2) the 2-D model using Fourier reduction; (3) Zener's analytical approximation; (4) Lifshitz and Roukes' analytical solution. By varying the beam thickness, different values for ξ were obtained corresponding to different Q-factors of vibration. The results were normalized against the terms originally introduced by Zener and Lifshitz. Clearly, close agreements have been achieved among all these models, despite slight differences observed between the numerical and analytical solutions. Overall, the Fourier model yields better predictions compared to the non-Fourier models, since the Fourier model was discretized into 50 elements across the thickness direction in the computation (note that the discretization in the longitudinal direction is not needed in the Fourier model), whereas only five elements across thickness was used in the non-Fourier model for reducing the computational effort. Note that both dimensions need to be discretized in a non-Fourier model and the element number is more important in the length direction than in the thickness direction. Computational results revealed that for a 2-D beam problem, using the Fourier model can reduce

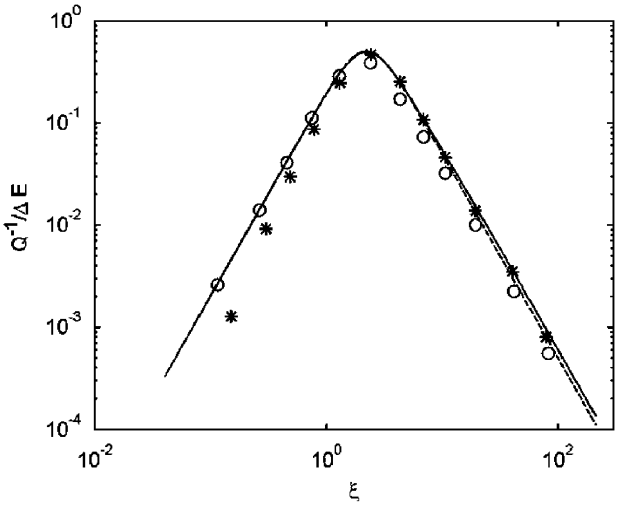

Fig. 2. Comparison between the finite element models and the analytical solutions for the quality factor of a thin beam ((—) Lifshitz's solution; (- - -) Zener's solution; (*) finite element 2-D non-Fourier model; (o) finite element 2-D Fourier model).

the finite element computational time by as much as 150–200 times assuming that only 30 elements (which is nearly the minimum number to ensure accuracy) are used in the longitudinal direction of the non-Fourier model!

The mild deviation of the Fourier model from the analytical solutions at large ξ (i.e., at large thickness) is a result caused by the difference between the beam theory and the theory of elasticity when the thickness is considerably large and comes close to the wave length of the resonance. In general, the results obtained from the Fourier finite element model (that is constructed from the theory of elasticity) are more accurate than the analytical solutions as well as the non-Fourier finite element models.

The 3-D axisymmetric Fourier model for an annular ring resonator has been validated by comparing the two limiting cases of ring geometry (with either very small radial width or very small axial thickness) to the 2-D Fourier model, as shown in Fig. 3. The rationale behind this comparison is that, when the ring is sufficiently thin in either direction, the curvature effect should be negligible and the results should approach the 2-D scenarios. In the case of small radial width, the in-plane modes will dominate; in the case of small axial thickness (in the z-direction), the out-of-plane modes will dominate. The material and geometric properties used in the computation are listed in Table 1. These parameters represent the properties of silicon resonators and were adapted from Wong et al.'s work [8]. In Fig. 3, the resonant eigenfrequency and quality factor have been presented as functions of wavenumber n along the circumference. Agreements have been observed for both frequency and Q-factor, especially when the wavenumber is large. When the wavenumber is small, for example $n<5$, the geometric effects become important. Therefore, the quality factor predicted from the 2-D Fourier model noticeably deviates from the 3-D models at small n, although the resonant frequency is nearly identical among different models.

To further explore the effect of the 3-D geometry on the relevant results, the radial width of the annular ring was varied while the mean radius maintained as the same. In this case, the difference between the inner and outer radii certainly imposes constraints on the mode shape of resonance. The numerical results presented in Fig. 4 apparently show that the radial width has significant effects on both the resonant frequency and the Q-factor. When the radial width varies between 0 and 6 mm, there is a maximum 90% difference of change in the resonant frequency and the variation in the Q-factor is about 10–15%. Also, the frequency exhibits a bell-shape relationship with the radial width: it increases at the beginning and then reaches a maximum value before it starts to decrease. These results illustrate that using a 2-D model to approximate a 3-D ring resonator could induce significant errors when the radial width is at the scale of ring diameter.

It should be noted that in the annular ring problem there exist multiple eigenmodes associated with each wavenumber n. Each of the modes has its own frequency of vibration as well as Q-factor. Fig. 5 displays the

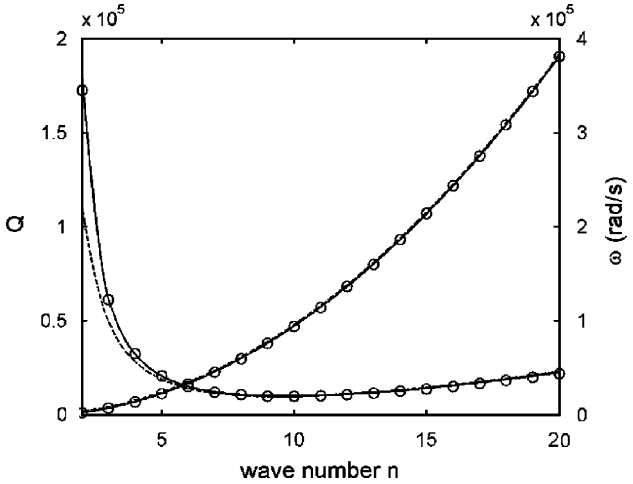

Fig. 3. Comparison between the two-dimensional Fourier model and the three-dimensional model in the limiting cases, where the radial or axial thickness is sufficiently small ((o) 3-D model with small radial width; (—) 3-D model with small z-thickness; (- - -) 2-D Fourier model; curves crossing the origin, frequency ω; curves not crossing the origin, Q-factor).

Table 1
Material and geometric properties

Young's modulus, E (Pa)	1.61×10^{11}
Poisson's ratio	0
Thermal expansion coefficient, α (K^{-1})	2.6×10^{-5}
Thermal conductivity, K ($W\,m^{-1}\,K^{-1}$)	141
Specific heat ($m^2\,s^{-1}$)	704
Density, ρ ($kg\,m^{-3}$)	2330
Temperature (K)	300
z-thickness (μm)	100
Mean ring radius (mm)	5

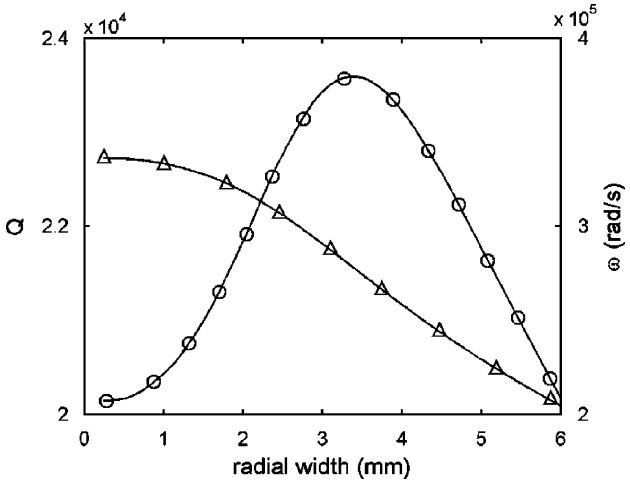

Fig. 4. Resonant frequency and Q-factor of the dominant mode (i.e. the out-of-plane mode with the lowest resonant frequency) as functions of radial width ((o) frequency ω; (Δ) Q-factor).

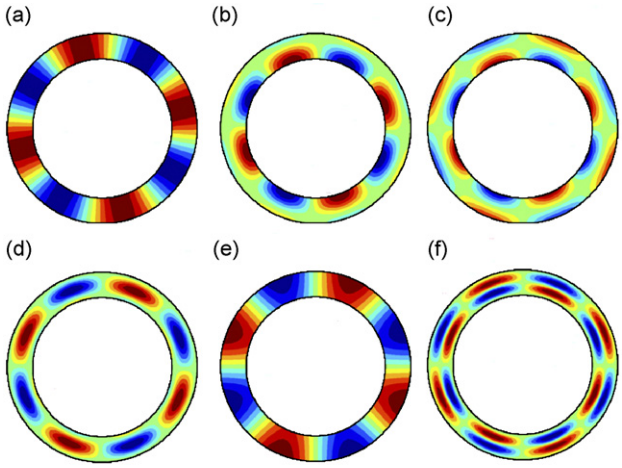

Fig. 5. Dominant out-of-plane eigenmodes in the form of contour plots of surface temperature field for wavenumber $n = 4$ in a ring resonator. The resonant frequency in (1) through (6) is corresponding to mode 1 through 6 in Table 2.

mode shape patterns (eigenvectors) for the leading modes at $n = 4$, visualized as the contour plots of the temperature field on the ring surface. It is interesting to notice that there could be several reversals across the radius, as shown in Fig. 5(6), but these modes typically have higher resonant frequencies. The values of the

Table 2
Frequencies and Q-factors of the leading modes for $n = 4$ in the ring model

Mode #	Frequency (rad s^{-1})	Q-factor
1	1.400×10^5	1.188×10^4
2	6.810×10^5	1.998×10^5
3	1.829×10^6	1.928×10^7
4	3.213×10^6	2.613×10^5
5	6.752×10^6	5.793×10^8
6	8.212×10^6	6.257×10^5

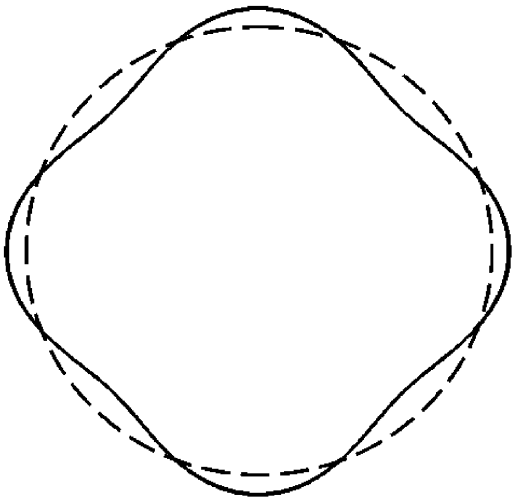

Fig. 6. The in-plane vibration mode for $n = 4$ when the radial width is much smaller than the axial z-thickness ((—) deformed shape; (- - -) undeformed shape).

frequencies along with the Q-factors are tabulated in Table 2. It has been noticed that the quality factors may differ by four orders of magnitude among the six dominant modes despite their close resonant frequencies. The large products of frequency and Q-factor (approximately on the order of magnitude 10^{15}) in some of the modes imply that minimization of thermoelastic energy loss is possible at high resonant frequencies via exciting certain types of eigenmodes (this could probably be achieved by imposing certain boundary constraints). The physical relationships between these mode shapes and the variations in the Q-factors are not yet known and rely on future investigations. The 3-D distributions of the corresponding displacement or velocity fields for the dominant modes can also be obtained. But they exhibit the same profiles compared to the temperature distribution and thus are not presented here.

When the radial width were sufficiently small (e.g. smaller than the axial thickness), the resonance would involve in-plane modes only, as shown in Fig. 6. This case was discussed in great details in Wong et al.'s work [8] and obviously it is a special case of the generalized annular ring model studied in the present work. Compared to the out-of-plane modes, the in-plane modes do not have complicated patterns as the out-of-plane modes, due to the geometric homogeneity in the ring's axial direction (z-direction).

8. Conclusions

The effects of geometry on thermoelastic damping have been investigated by comparing the finite element results from the 2-D and 3-D models. The application of the Fourier reduction method greatly simplifies the solution procedure in both geometries. Specifically, by prescribing a Fourier number, a 2-D layer model can be reduced to a problem defined on the thickness direction, thus requiring finite element meshing on one

dimension only; likewise, the 3-D ring model can be reduced to a problem defined on the 2-D cross section of the geometry and thus the discretization is required on a plane domain only. The method has been validated via comparing the finite element results from the 2-D thin beam model with the existing analytical solutions found in the literature. The effect of the radial width in the ring problem has also been investigated by using the 3-D Fourier model. It has been shown that the curvature in the geometry is an important contributing variable for both the resonant frequency and the quality factor when either the wave length or the radial width is sufficiently large. The 3-D model also exhibits characteristics different from the 2-D model, such as the multiple mode shape patterns corresponding to each of the Fourier numbers. Although the analyses in this study are relevant to the symmetric geometries, the same method can be readily extended to other problems. When the symmetry is absent either in the geometry or in the boundary condition, however, the Fourier reduction method will fail and a general 3-D formulation must be used instead.

References

[1] T.V. Roszhart, The effect of thermoelastic internal friction on the Q of micromachined silicon resonators, *Proceedings of the IEEE Solid-State Sensors Actuator Workshop Fourth Technical Digest*, IEEE, New York, 1990, pp. 13–16.

[2] S. Evoy, A. Olkhovets, L. Sekaric, J.M. Parpia, H.G. Craighead, D.W. Carr, Temperature-dependent internal friction in silicon nanoelectromechanical systems, *Applied Physics Letters* 77 (2000) 2397–2399.

[3] R. Abdolvand, G.K. Ho, A. Erbil, F. Ayazi, Thermoelastic damping in trench-refilled polysilicon resonators, Transducers '03 Digest of Technical Papers, Vol. 1, June 2003, pp. 324–327.

[4] Z.F. Khisaeva, M. Ostoja-Starzewski, Thermoelastic damping in nanomechanical resonators with finite wave speeds, *Journal of Thermal Stresses* 29 (2006) 201–216.

[5] C. Zener, Internal friction in solids I: theory of internal friction in reeds, *Physical Review* 52 (1937) 230–235.

[6] R. Lifshitz, M.L. Roukes, Thermoelastic damping in micro- and nanomechanical systems, *Physical Review B* 61 (2000) 5600–5609.

[7] A.H. Nayfeh, M.I. Younis, Modeling and simulations of thermoelastic damping in microplates, *Journal of Micromechanics and Microengineering* 14 (2004) 1711–1717.

[8] S.J. Wong, C.H.J. Fox, S. McWilliam, Thermoelastic damping of the in-plane vibration of thin silicon rings, *Journal of Sound and Vibration* 293 (2006) 266–285.

[9] A. Duwel, J. Gorman, M. Weinstein, J. Borenstein, P. Ward, Experimental study of thermoelastic damping in MEMS gyros, *Sensors and Actuators A* 103 (2003) 70–75.

[10] B.H. Houston, D.M. Photiadis, M.H. Marcus, J.A. Bucaro, X. Liu, J.F. Vignola, Thermoelastic loss in microscale oscillators, *Applied Physics Letters* 80 (2002) 1300–1302.

[11] X. Liu, J.F. Vignola, H.J. Simpson, B.R. Lemon, B.H. Houston, D.M. Photiadis, A loss mechanism study of a very high Q silicon micromechanical oscillator, *Journal of Applied Physics* 97 (2005) Art No. 023524.

[12] Y. Guan, M.A. Matin, Design and analysis of MEM-micromirrors for vertical cavity surface emitting lasers, *Microwave and Optical Technology Letters* 37 (2003) 410–413.

[13] Y. Guan, M.A. Matin, Dynamic behavior of MEM-mirrors for tunable-VCSELs, *Microwave and Optical Technology Letters* 39 (2003) 203–207.

[14] J.P. Gorman, Finite Element Analysis of Thermoelastic Damping in MEMS, MS Thesis, Department of Materials Science and Engineering, Massachusetts Institute of Technology, May 2002.

[15] M.J. Silver, L.D. Peterson, Predictive elastothermodynamic damping in finite element models by using a perturbation formulation, *AIAA Journal* 43 (2005) 2646–2653.

[16] Y.B. Yi, J.R. Barber, P. Zagrodzki, Eigenvalue solution of thermoelastic instability problems using Fourier reduction, *Proceedings of the Royal Society of London Series A: Mathematical and Physical Sciences* 456 (2000) 2799–2821.

[17] Y.B. Yi, Finite element analysis on thermoelastodynamic instabilities involving frictional heating, *ASME Journal of Tribology* 128 (2006) 718–724.

[18] O.C. Zienkiewicz, R.L. Taylor, *The Finite Element Method*, fifth ed., Butterworth-Heinemann, Oxford, 2000.